A Comparison of the Isotope Effect for the N + N2 Reaction Calculated on Two Potential Energy Surfaces

CONFERENCE PAPER · JUNE 2008

DOI: 10.1007/978-3-540-69839-5_82 · Source: DBLP

4 AUTHORS:

Sergio Rampino
Consiglio Nazionale delle Ricerche, Italy
32 PUBLICATIONS **134** CITATIONS
SEE PROFILE

Dimitrios Skouteris
Scuola Normale Superiore di Pisa
68 PUBLICATIONS **1,191** CITATIONS
SEE PROFILE

Antonio Laganà
Università degli Studi di Perugia
162 PUBLICATIONS **1,046** CITATIONS
SEE PROFILE

Ernesto Garcia
Universidad del País Vasco / Euskal Herriko…
93 PUBLICATIONS **1,137** CITATIONS
SEE PROFILE

A Comparison of the Isotope Effect for the $N + N_2$ Reaction Calculated on Two Potential Energy Surfaces

Sergio Rampino[1], Dimitris Skouteris[1], Antonio Laganà[1], and Ernesto Garcia[2]

[1] Dipartimento di Chimica, Università di Perugia,
Via Elce di Sotto 8, 06123 Perugia, Italy
{ser_ram,dimitris,lag}@dyn.unipg.it
[2] Departamento de Quimica Fisica, Universidad del Pais Vasco,
Paseo de la Universidad 7, 01006 Vitoria, Spain
e.garcia@ehu.es

Abstract. The atom-diatom time independent quantum reactive scattering program ABC implemented on the COMPCHEM section of the EGEE computing Grid has been used to compute isotope effects for the nitrogen atom - nitrogen molecule reactions. Exact $J = 0$ quantum scattering calculations were performed for both the $^{14}N + {}^{28}N_2$ and $^{14}N + {}^{30}N_2$ reactions on two different potential energy surfaces. Related reaction thresholds, reactive resonances and product distributions are discussed. J-shifting thermal rate coefficients are also calculated for a comparison with the experiment.

Keywords: reactive scattering, quantum dynamics and kinetics, nitrogen exchange reaction, reactive resonances, isotope effect.

1 Introduction

The exchange and dissociation reactions of nitrogen atom - nitrogen molecule systems play a primary role in the modeling of spacecraft reentry [1]. Both the heat load and the reactivity of the species produced by the shock wave are, in fact, important data for heat shield design since nitrogen is the largest component of Earth's atmosphere. Reactions of nitrogen are also important in other high temperature environments involving N_2, as, for example, shock tube experiments [2].

We focus our attention here on the following isotopic variants of the nitrogen atom - nitrogen molecule reaction

$$^{14}N(^4S) +^{28} N_2(^1\Sigma_g^+, v, j) \rightarrow^{28} N_2(^1\Sigma_g^+, v', j') +^{14} N(^4S) \quad (1)$$

$$^{14}N(^4S) +^{30} N_2(^1\Sigma_g^+, v, j) \rightarrow^{29} N_2(^1\Sigma_g^+, v', j') +^{15} N(^4S), \quad (2)$$

in order to evaluate the effect of changing the mass of the reactants on detailed (such as state to state probabilities $P_{vj,v'j'}(E_{tr})$, with E_{tr} being the relative

O. Gervasi et al. (Eds.): ICCSA 2008, Part I, LNCS 5072, pp. 1081–1093, 2008.

atom-diatom collision energy and vj ($v'j'$) the vibrotational state of reactants (products)) and more averaged (such as thermalized reaction rate coefficients $k(T)$, with T being the temperature) dynamical properties.

The computational study of reactions 1 and 2 is also important from a theoretical point of view. In particular, it is useful to the end of assessing the role played by internal and translational motions in promoting reactivity for non light systems.

In our study we used the time independent quantum reactive scattering program ABC [3] to perform exact $J = 0$ fixed total energy (E) quantum calculations on two different potential energy surfaces (PESs). Calculations were performed for such an extended fine grained interval of energy values to allow not only a careful investigation of mentioned dynamical effects but also the accurate evaluation of the thermal rate coefficient using $J = 0$ exact quantum probabilities [4]. This highly demanding computational task was made possible by the distribution of the jobs to run among the CPUs of the section of the production computing grid of EGEE [5] accessible to the COMPCHEM [6] virtual organization.

In section 2 a brief description of the computational procedure is given. The two potential energy surfaces used in the calculations are illustrated in sections 3 and 4. Section 5 is devoted to the discussion of the results. Some conclusions are drawn in the last section.

2 Computational Procedure

The program ABC uses a time independent hyperspherical coordinate method [7] to solve the atom-diatom Schrödinger equation for a reaction occurring on a single PES within a Born-Oppenheimer scheme. In the Born-Oppenheimer scheme the Schrödinger equation of the nuclei reads

$$[\hat{H} - E]\psi = 0, \tag{3}$$

with ψ being the nuclear wavefunction (depending on nuclear coordinates only) and $\hat{H}$ being the related electronically adiabatic Hamiltonian.

In the approach adopted by ABC ψ is expanded in terms of the hyperspherical arrangement channel (τ) basis functions $B^{JM}_{\tau v_\tau j_\tau \Omega_\tau}$ which are labeled after J (the total angular momentum quantum number), M and Ω_τ (the space- and body-fixed projections of the total angular momentum $\mathbf{J}$), v_τ and j_τ (the τ asymptotic vibrational and rotational quantum numbers), and depend on both the three Euler angles and the internal Delves hyperspherical angles. In order to carry out the propagation of the solution from small to asymptotic values of the ρ reaction coordinate ($\rho = (R_\tau^2 + r_\tau^2)^{1/2}$, with $\mathbf{R}_\tau$ and $\mathbf{r}_\tau$ being the Jacobi vectors forming the angle Θ_τ and R_τ and r_τ the related moduli) we need to integrate the equations

$$\frac{\mathrm{d}^2\mathbf{g}(\rho)}{\mathrm{d}\rho^2} = \mathbf{S}^{-1}\mathbf{U}\mathbf{g}(\rho), \tag{4}$$

where $\mathbf{g}(\rho)$ is the matrix of the coefficients of the expansion of ψ, $\mathbf{S}$ is the overlap matrix defined as

$$S^{\tau v'_\tau j'_\tau \Omega'_\tau}_{\tau v_\tau j_\tau \Omega_\tau} = \langle B^{JM}_{\tau v_\tau j_\tau \Omega_\tau} | B^{JM}_{\tau v'_\tau j'_\tau \Omega'_\tau} \rangle, \tag{5}$$

and $\mathbf{U}$ is the coupling matrix defined as

$$U^{\tau v'_\tau j'_\tau \Omega'_\tau}_{\tau v_\tau j_\tau \Omega_\tau} = \langle B^{JM}_{\tau v_\tau j_\tau \Omega_\tau} | \frac{2\mu}{\hbar^2}(\bar{H} - E) - \frac{1}{4\rho^2} | B^{JM}_{\tau v'_\tau j'_\tau \Omega'_\tau} \rangle, \tag{6}$$

with μ being the reduced mass of the system and $\bar{H}$ the set of terms of the Hamiltonian not containing derivatives with respect to ρ.

To integrate eq. 4 we divide the ρ interval into various sectors, and solve for local (sector) bound state functions by diagonalizing a fixed Θ_τ Hamiltonian using a carefully chosen reference potential. Coupled-channel equations, generated by expanding the solution in terms of the sector local bound functions, are then integrated inside each sector and through all of them.

3 The L3 Potential Energy Surface

A LEPS formulation of the N + N_2 PES was the first to appear in the literature [8]. Such PES has a saddle to reaction associated with a symmetric collinear ($\hat{\text{NNN}} = 180°$) geometry. The *ab initio* finding of a bent ($\hat{\text{NNN}} \simeq 120°$) geometry at the saddle to reaction was reported in refs. [9,10]. This proved the inadequacy of the LEPS PES to describe correctly the main features of the strong interaction region of the reaction channel and motivated us to develop a new functional representation of the PES called LAGROBO (Largest Angle Generalization of the ROtating Bond Order) [11].

The LAGROBO functional (V^{LAGROBO}) is built out of a combination of the ROtating Bond Order (ROBO) [12] V^{ROBO}_τ model potentials associated with the description of the various (τ) exchange processes allowed for the considered system[1]. Accordingly the LAGROBO PES is formulated as

$$V^{\text{LAGROBO}}(r_{\tau,\tau+1}, r_{\tau+1,\tau+2}, r_{\tau+2,\tau}) = \sum_\tau w(\Phi_\tau) V^{\text{ROBO}}_\tau(\rho_\tau, \alpha_\tau, \Phi_\tau), \tag{7}$$

where ρ_τ is the hyperradius of the hyperspherical BO (HYBO) coordinates defined as $\rho_\tau = (n^2_{\tau+2,\tau} + n^2_{\tau,\tau+1})^{1/2}$, and $\alpha_\tau = \arctan[n_{\tau,\tau+1}/n_{\tau+2,\tau}]$ (where $n_{\tau,\tau+1} = \exp[-\beta_{\tau,\tau+1}(r_{\tau,\tau+1} - r_{e\tau,\tau+1})]$ is the BO coordinate of the $\tau, \tau+1$ diatom with the process index τ being cyclic of module 3 and indicating the exchanged atom). In eq. 7 $w(\Phi_\tau)$ is a weight function that privileges the ROBO potential better representing the overall interaction as the related Φ_τ (the angle formed by the two (broken and formed) bonds having in common the atom τ) varies [12,13]. The weighting coefficient $w(\Phi_\tau)$ is defined as

$$w(\Phi_\tau) = \frac{u(\Phi_\tau)}{\sum_\tau u(\Phi_\tau)}, \tag{8}$$

[1] It is important to emphasize here the different meaning of τ in eqs. 5 and 6, where it labels the arrangement channel, as opposed to its meaning here as exchanged atom label. It is worth noting also the different definition of ρ_τ.

with $u(\Phi_\tau)$ being a damping function of the type

$$u(\Phi_\tau) = \frac{1}{2}\left(1 + \tanh\left[\gamma_\tau(\Phi_\tau - \Phi_\tau^\circ)\right]\right). \tag{9}$$

Since the three reaction channels are all of the type N + N_2, whenever possbile we drop the subscript τ. Accordingly, we have the same values for γ and Φ° (50 and 75°) for all channels. The functional representation of the ROBO potential is

$$V^{\mathrm{ROBO}}(\rho, \alpha, \Phi) = a_1(\alpha, \Phi)\left[2\frac{\rho}{a_2(\alpha, \Phi)} - \frac{\rho^2}{a_2^2(\alpha, \Phi)}\right]. \tag{10}$$

The function $a_1(\alpha, \Phi)$ describes the dependence of the well depth of the fixed Φ minimum energy path (MEP) of the exchange process, while the function $a_2(\alpha, \Phi)$ describes the location on ρ of the minimum of the fixed Φ MEP of the exchange process.

In this way an alternative PES called L3 [14], was formulated by defining $a_1(\alpha, \Phi) = -D_{\mathrm{N}_2} + b_{11}(\Phi)\sin(\alpha)$ and $a_2(\alpha, \Phi) = 1 + b_{21}(\Phi)\sin(2\alpha)$, where

$$b_{ij}(\Phi) = \sum_{k=1}^{4} c_{ijk}(\Phi_i^{\mathrm{TS}} - \Phi)^\zeta, \tag{11}$$

with $\zeta = k-1$ for $b_{1j}(\Phi)$ and $\zeta = 2(k-1)$ for $b_{2j}(\Phi)$. Because of the second order (Morse like) formulation of the ROBO model potential adopted here, $D_{\mathrm{N}_2} = 228.40$ kcal mol^{-1}, $\beta = 2.689$ Å^{-1}, and $r_{\mathrm{e}} = 1.0977$ Å. The values of the c_{ijk} parameters are given in table 1, while Φ_1^{TS} and Φ_2^{TS} were given the values of 125° and 180° respectively.

Table 1. Values of the c_{ijk} parameters for the L3 PES

c_{1jk}/kcal mol^{-1}		c_{2jk}/Å	
c_{111}	32.28	c_{211}	-0.0367
c_{112}	53.03	c_{212}	-0.0318
c_{113}	24.49	c_{213}	0.0064
c_{114}	24.73	c_{214}	-0.0059

The L3 PES has a saddle of 1.40 eV associated with a bent symmetric geometry as enforced by our choice of $\Phi_1^{\mathrm{TS}} = 125°$ (again the same for all τ values) and shown in the first column of table 2.

4 The L4 PES

More recently new high-level *ab initio* calculations have been performed for three thousand geometries of the N + N_2 system [15], and calculated values have been fitted using an umpublished functional form. Due to the impossibility of

Table 2. Features of the reaction channel of the L3 and L4 PESs. The prefix "i" labels the heavy isotope case.

	L3 PES s	L4 PES s	L4 PES w
r_{12}/bohr	2.37	2.24	2.40
r_{23}/bohr	2.37	2.77	2.40
Φ/degrees	125.0	116.7	118.6
V/eV	1.40	2.06	1.93
A/eV	6.7×10^{-4}	4.8×10^{-4}	
B/eV	6.0×10^{-5}	5.8×10^{-5}	
C/eV	5.5×10^{-5}	5.2×10^{-5}	
iA/eV	6.3×10^{-4}	4.5×10^{-4}	
iB/eV	5.8×10^{-5}	5.6×10^{-5}	
iC/eV	5.3×10^{-5}	5.0×10^{-5}	

reproducing the obtained PES (called WSHDSP from the initials of the authors), that exhibits two fairly high barriers sandwiching a shallow well, we calculated afresh a proper set of *ab initio* energies [16] and developed a new LAGROBO PES (L4) having similar characteristics.

Ab initio calculations of the electronic energy for the N + N_2 exchange reaction have been carried out using the open shell CCSD(T)/aug-cc-pVTZ method as implemented in the MOLPRO code [17]. Three sets of calculations were performed to obtain a good description of the transition state, a proper dependence on the bond angle Φ of both the geometry and the energy of the well sandwiched by the two barriers, and an accurate characterization of the MEPs at several bond angles Φ.

To enable L4 to reproduce the particular structure of the MEP of the *ab initio* data the a_1 function was given the formulation

$$a_1(\alpha, \Phi) = -D_{N_2} + b_{10}(\Phi) + b_{12}(\Phi)(\alpha - 45^\circ)^2 + \left(\frac{-b_{10}(\Phi) - b_{12}(\Phi)\ (45^\circ)^2}{(45^\circ)^4} \right) (\alpha - 45^\circ)^4, \tag{12}$$

where

$$b_{10}(\Phi) = c_{100} + c_{102}(\Phi - 118.6^\circ)^2 + c_{103}(\Phi - 118.6^\circ)^3 \tag{13}$$

and

$$b_{12}(\Phi) = c_{120} + c_{121}\Phi + c_{122}\Phi^2, \tag{14}$$

while the a_2 function was given the formulation

$$a_2(\alpha, \Phi) = +b_{20}(\Phi) + b_{22}(\Phi)(\alpha - 45^\circ)^2 + \left(\frac{3 - 3\ b_{20}(\Phi) - 2\ b_{22}(\Phi)\ (45^\circ)^2}{(45^\circ)^4} \right) (\alpha - 45^\circ)^4 + \left(\frac{-2 + 2\ b_{20}(\Phi) + b_{22}(\Phi)\ (45^\circ)^2}{(45^\circ)^6} \right) (\alpha - 45^\circ)^6, \tag{15}$$

where

$$b_{20}(\Phi) = c_{200} + c_{201}\Phi + c_{202}\Phi^2 + c_{203}\Phi^3 \tag{16}$$

and

$$b_{22}(\Phi) = c_{220} + c_{221}\Phi + c_{222}\Phi^2. \tag{17}$$

The values of the c_{ijk} parameters of the L4 PES are given in table 3 (the values of the other parameters are the same as for L3).

Table 3. Values of the c_{ijk} parameters for the L4 PES

c_{1jk}/kcal mol^{-1}		c_{2jk}/Å	
c_{100}	44.517	c_{200}	-1.6614
		c_{201}	0.049931
c_{102}	0.0313099	c_{202}	-3.1748E-4
c_{103}	-0.000291921	c_{203}	6.5962E-7
c_{120}	-0.15084	c_{220}	2.5469E-3
c_{121}	0.0024633	c_{221}	-3.9557E-5
c_{122}	-8.9852E-6	c_{222}	1.4342E-7

The properties of the L4 PES are illustrated in the second and third columns of table 2, where the geometry and the potential energy V of the system at the saddles (labeled by s) and at the bottom of the intermediate well (labeled by w) are reported together with the rotational constants of $^{14}N^{14}N^{14}N$ and $^{14}N^{15}N^{15}N$ at the saddle geometries. Please note that the geometry of the system at the L4

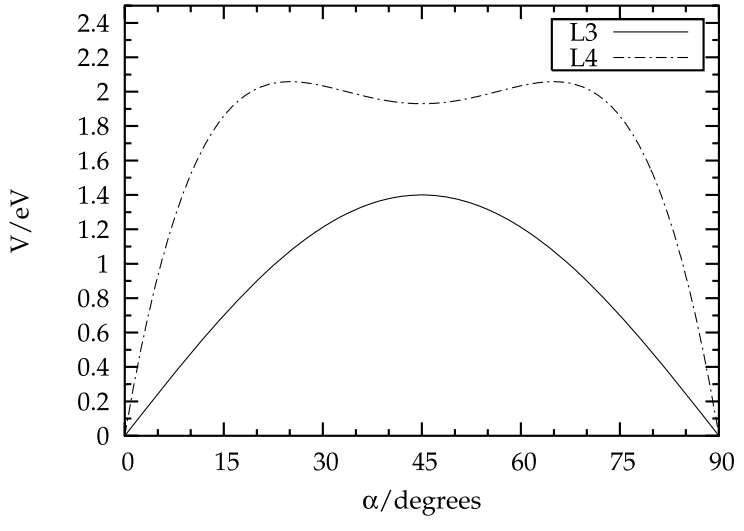

Fig. 1. Minimum energy path for the L3 (solid line) and the L4 (dashed-dotted line) PESs plotted as a function of the HYBO hyperangle α

saddle ($V_s = 2.06$ eV) is asymmetric ($r_{s12} = 2.24$ bohr, $r_{s23} = 2.77$ bohr) while at the bottom of the well it is symmetric ($r_{w12} = r_{w23} = 2.40$ bohr and $V_w = 1.93$ eV) Accordingly, the depth of the well is 0.13 eV.

To further illustrate the properties of both L3 and L4, related MEPs are plotted in fig. 1 as a function of the HYBO hyperangle α. The different structure of the two PESs is apparent.

5 Results and Discussion

As already mentioned, we carried out exact quantum scattering calculations for the reactions of ^{14}N with both $^{28}N_2$ and $^{30}N_2$ (as specified by the three values of `mass` in table 4) on the L3 and L4 PESs. The calculations were performed at null total angular momentum (`jtot` of table 4) and diatomic parity (`jpar`) equal to 1 (that means including only odd reactant rotational levels).

For L3 the investigated interval of total energy was varied from 1.2 eV (indicated by the value of `enrg`), some tenths of eV below the barrier, up to 3.1 eV, about two times the energy of the barrier, using a grid (`nnrg`) of 153 total values having an energy step (`dnrg`) of 0.0125 eV. The maximum internal energy (`emax`) was set equal to 3.5 eV. To include all the asymptotically open channels a large maximum rotational quantum number (`jmax`) should have been considered. However, since the value of the computed probabilities does not show any significant change if channels with j larger than 75 are neglected, we truncated accordingly the number of rotational functions used in the expansion. Convergence tests suggested to choose an upper value of the hyperradius (`rmax`) of 12.0 bohr.

Due to the higher reaction barrier, for L4 the minimum value of the total energy was set at 2.0 eV (just below the barrier) and the maximum one at 4.1 eV (about two times the energy of the barrier), with a maximum internal energy set equal to 4.5 eV.

Table 4. Input parameters for the calculations carried out on the reaction N + N_2 using L3 and L4 PESs. `mtr` is the number of log derivative propagation sectors.

Parameter	L3	L4
`mass =`	`14.00674,15.00011,15.00011`	`14.00674,15.00011,15.00011`
`jtot =`	`0`	`0`
`jpar =`	`1`	`1`
`emax =`	`3.5`	`4.5`
`jmax =`	`75`	`75`
`rmax =`	`12.0`	`12.0`
`mtr =`	`150`	`150`
`enrg =`	`1.2`	`2.0`
`dnrg =`	`0.0125`	`0.0125`
`nnrg =`	`153`	`169`

5.1 Threshold and Reactive Resonances

State specific reactive probabilities have been plotted in fig. 2 as a function of relative kinetic energy for the vibrotational ground state of the reactant molecule $^{28}N_2$ and $^{30}N_2$ on both the L3 and L4 PESs. In all figures the prefix "i" in the keybox refers to the case of the heavier N isotope of the reactant molecule (reaction 2).

The thresholds calculated on both surfaces for reactions 1 and 2 are clearly different with that for L4 being much higher than the one for the L3 PES (in agreement with its higher barrier) though no isotope effect is found.

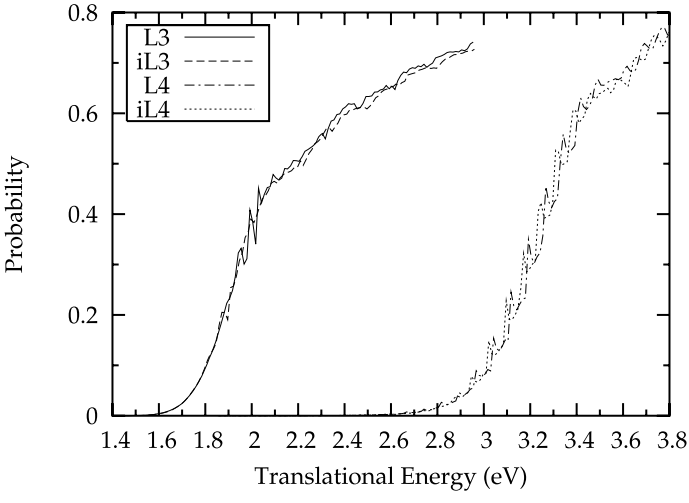

Fig. 2. Reactant vibrotational ground state reaction probabilities calculated on the L3 PES for the reaction of ^{14}N with $^{28}N_2$ (solid line) and $^{30}N_2$ (dashed line) and on the L4 PES (dashed-dotted line, dotted line). In the key box, the prefix "i" labels the heavy isotope case.

Another important difference between the two sets of results is the resonant structure. The dependence on collision energy of the reactive probability calculated for reaction 1 (solid line of the left hand side curves of fig. 2) on L3, is fairly smooth apart from a series of a few small peaks located around $E_{\rm tr} = 2$ eV (which are further smoothed for the heavier isotope). Reactive probabilities calculated on L4 show instead a regular resonance structure (several peaks with spacing of 0.075 eV and some shoulders) for both isotopic variants though with a small shift in going from reaction 1 to reaction 2.

A similar structure was found in ref. [18] for the reaction probability calculated on the WSHDSP PES for the transition from $v = 0$, $j = 0$ to $v' = 0$, $j' = 0$. As in the WSHDSP case, the quasibound bending states supported by the well are associated with the resonance peaks, while the shoulders are associated with the stretching quasibound states.

Clearly, the quite confined resonance effect found on the L3 cannot be due to the trapping in a potential energy minimum (absent on this PES). It is instead of pure dynamical origin. This is confirmed by the fact that (as shown in fig. 2) the isotopic variation wipes out the structure obtained on L3 while that obtained on L4 keeps its regular energy shifted structure.

5.2 Product Vibrational and Rotational Distributions

Zero total angular momentum and rotational quantum numbers product vibrational distributions (PVDs) were calculated at a relative kinetic energy of 1.65 eV and $v = 0$, 1, 2 for both reactions 1 and 2 on the L3 PES. The PVDs calculated on the L3 PES and normalized to the maximum are shown in the left hand side panels of fig. 3 as a function of the product vibrational quantum number v'. The plots show that on L3 the reactive processes are mainly adiabatic with the exception of $v = 1$, for which a strong deexcitation to $v' = 0$ is observed. Such an exception has been rationalized elsewhere [4]. No significant isotope effect is found in the product vibrational distribution.

Similar calculations were performed on L4 at a relative kinetic energy of 2.40 eV. Relevant results are shown in the right hand side panels of fig. 3. The plots show that the reactive process for both isotopic variants is mostly adiabatic for $v = 0$ while it is strongly non adiabatic for $v = 1$ and 2, for which deexcitation to $v' = 0$ is the major process. Moreover, a significant vibrational excitation of the products is found. Also the isotope variation significantly affects the product vibrational distribution.

Calculations were repeated for both reactions 1 and 2 by selecting a value of the relative kinetic energy correponding to a peak and a slightly lower one. Related PVDs are shown in the right hand side and left hand side panels of fig. 4, respectively. In both cases no significant isotope effect is found.

5.3 Thermal Rate Coefficients

Due to the large number of involved partial waves, even for moderately heavy systems (like the N + N_2 considered here), the calculation of the rate coefficient is very often carried out by adopting the popular J-shifting model [19,20], in which $J = 0$ probabilities ($P^{J=0}(E)$) are shifted in energy to approximate the higher J ones ($P^{J\Omega}(E)$) as follows:

$$P^{J\Omega}(E) = P^{J=0}(E - \Delta E^{J\Omega}), \tag{18}$$

with $\Delta E^{J\Omega}$ being defined as

$$\Delta E^{J\Omega} = \bar{B}J(J+1) + (A - \bar{B})\Omega^2. \tag{19}$$

This formula is based on the approximation that the geometry of the system at the bent saddle is a symmetric top one. In eq. 19 $\bar{B} = (B + C)/2$ with A, B and C being the three rotational constants of the triatom at the saddle given

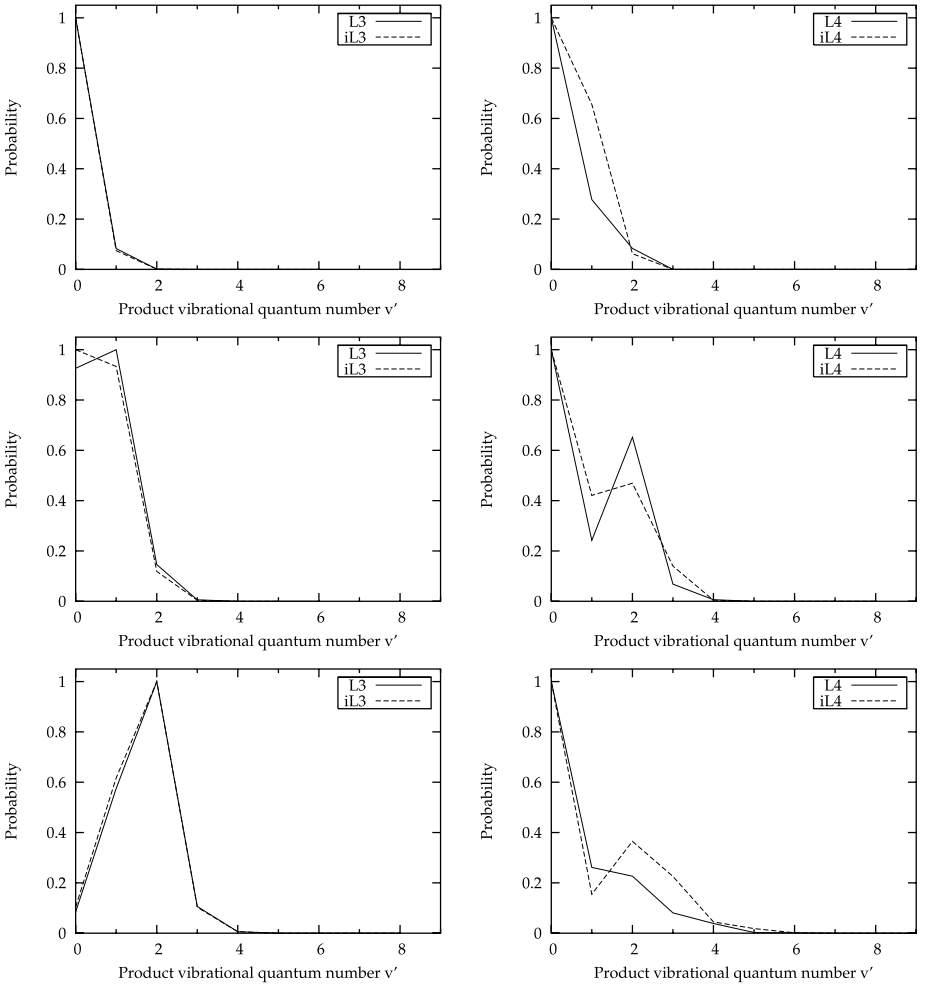

Fig. 3. Product vibrational distributions calculated on the L3 PES at $E_{\rm tr} = 1.65$ eV, $v = 0$ (upper panels), 1 (central panels), 2 (lower panels) and $j = J = 0$ plotted as a function of the product vibrational state v' for reaction 1 (solid line) and 2 (dashed line) in the left hand side column. The corresponding plots calculated on the L4 PES at $E_{\rm tr} = 2.40$ are given in the right hand side panels. Distributions are normalized to the maximum.

in table 2. In the J-shifting approximation the thermal rate coefficient can be written as

$$k(T) = \frac{1}{hQ_{\rm R}} \sum_{J=0}^{\infty} (2J+1) \sum_{\Omega=-J}^{J} \int_0^{\infty} e^{-E/k_{\rm B}T} \sum_{v,j} \sum_{v',j'} P^{J=0}_{vj\to v'j'}(E - \Delta E^{J\Omega})\, {\rm d}E, \tag{20}$$

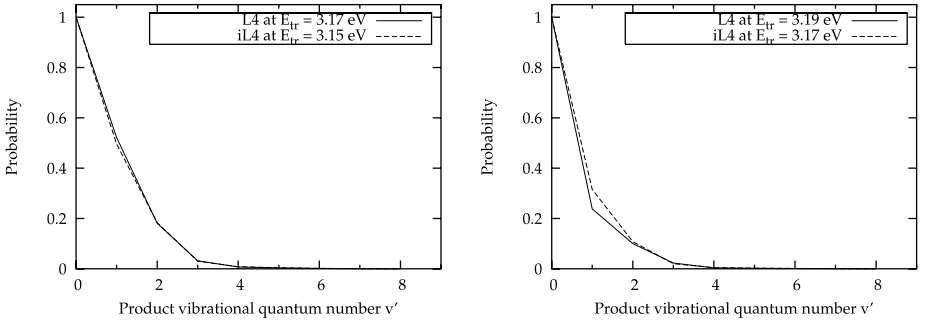

Fig. 4. Product vibrational distributions calculated on the L4 PES at $v = 0$ and $j = J = 0$ for a non resonant (left hand side panel) and a resonant (right hand side panel) kinetic energy plotted as a function of the product vibrational state v' for reaction 1 (solid line) and 2 (dashed line). Distributions are normalized to the maximum.

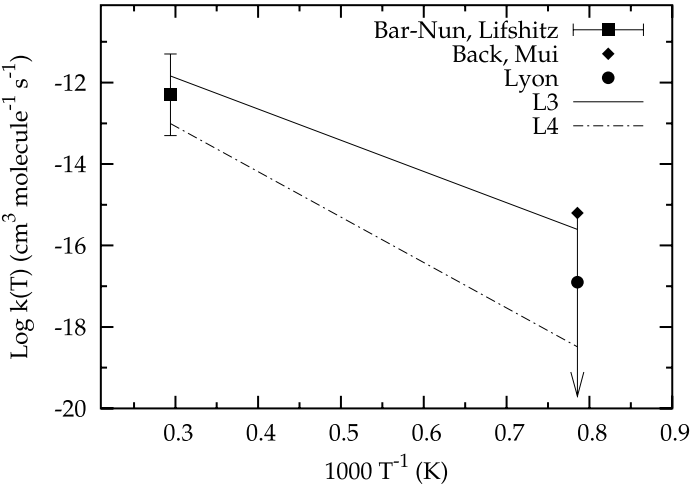

Fig. 5. Logarithm of the rate coefficient for the exchange reaction on L3 and L4 PESs plotted as a function of the inverse temperature using the J-shifting model of eq. 20. Experimental data of refs. [21,22,23] are also shown. Note that experiments at $T = 1273$ K only give upper limits for the rate coefficient.

where h is Planck's constant and Q_{R} is the total atom-diatom partition function of the reactants at temperature T per volume unit defined as

$$Q_{\mathrm{R}} = \left(\frac{2\pi\mu_{N,N_2}k_{\mathrm{B}}T}{h^2}\right)^{3/2}\left(\sum_{v,j}(2j+1)e^{-\epsilon_{vj}/k_{\mathrm{B}}T}\right). \qquad (21)$$

Experimental values of the rate coefficient of the N + N_2 reaction at temperatures of 1273 K (only as upper limits) and 3400 K are given in refs. [21,22,23]. The values of the rate coefficients of the $^{14}N + {}^{28}N_2$ and $^{14}N + {}^{30}N_2$ reactions calculated at the temperatures of the experiment on the L3 and L4 surfaces are the same in spite of the fact that some previously discussed more detailed quantities differ significantly. On the contrary, as shown by the plot of $\log k(T)$ versus $1/T$ of figure 5, the rate coefficients calculated on the L3 and L4 PESs (though falling both within the experimental error bars) differ significantly, with the former being higher than the latter, in agreement with the much lower barrier of the L3 PES. Furthermore, rate coefficients calculated on L4 have a sharper dependence on the temperature.

6 Conclusions

In this work we carried out time independent quantum scattering calculations for two isotope variants of the reactive system N + N_2 on two different potential energy surfaces. The large computational effort associated with this task has benefitted from the Grid implementation of related programs.

The calculations singled out a marked isotope effect on the location of the reactive resonances in $v = j = J = 0$ initial state selected probabilities obtained on L4. This is linked to the presence in L4 of a well placed on the top of the barrier. In contrast, the state selected probabilities calculated on L3 (that has no well) have a definitely smoother shape.

Another clear fingerprint of the dynamical importance of the intermediate well is the strong vibrational deexcitation effect shown by product vibrational distributions calculated on L4 that comes together with an evident isotope effect. Little vibrational deexcitation and isotope effect was instead found for L3.

Virtually no isotope effect was found for the calculated J-shifting thermal rate coeffcients (on both PESs), which were found to be in satisfactory agreement with the experimental data. This is particularly true for the J-shifting rate coefficient values calculated on L4, which not only fall within the error bars at $T = 3400$ K but also lie below the two experimental upper limits measured by the experiment at $T = 1273$ K.

References

1. Armenise, I., Capitelli, M., Celiberto, R., Colonna, G., Gorse, C., Laganà, A.: The effect of N+N_2 collisions on the non-equilibrium vibrational distributions of nitrogen under reentry conditions. Chem. Phys. Lett. 227, 157–163 (1994)
2. Armenise, I., Capitelli, M., Garcia, E., Gorse, C., Laganà, A., Longo, S.: Deactivation dynamics of vibrationally excited nitrogen molecules by nitrogen atoms. Effects on non-equilibrium vibrational distribution and dissociation rates of nitrogen under electrical discharges. Chem. Phys. Lett. 200, 597–604 (1992)
3. Skouteris, D., Castillo, J.F., Manolopoulos, D.E.: ABC: a quantum reactive scattering program. Comp. Phys. Comm. 133, 128–135 (2000)

4. Rampino, S.: Spacecraft reentry modeling: exact quantum calculations for the reaction N + N_2. Theoretical Chemistry and Computational Modeling European Master Thesis, Università di Perugia (2007)
5. Enabling Grids for E-Science in Europe, `http://www.eu-egee.org`
6. Laganà, A., Riganelli, A., Gervasi, O.: On the structuring of the computational chemistry Virtual Organization COMPCHEM. In: Gavrilova, M.L., Gervasi, O., Kumar, V., Tan, C.J.K., Taniar, D., Laganá, A., Mun, Y., Choo, H. (eds.) ICCSA 2006. LNCS, vol. 3980, pp. 665–674. Springer, Heidelberg (2006)
7. Schatz, G.C.: Quantum reactive scattering using hyperspherical coordinates: results for H + H_2 and Cl + HCl. Chem. Phys. Lett. 150, 92–98 (1988)
8. Laganà, A., Garcia, E., Ciccarelli, L.: Deactivation of vibrationally excited nitrogen molecules by collision with nitrogen atoms. J. Phys. Chem. 91, 312–314 (1987)
9. Petrongolo, C.: MRD-CI ground state geometry and vertical spectrum of N_3. J. Mol. Struct. 175, 215–220 (1988)
10. Petrongolo, C.: MRD-CI quartet potential surfaces for the collinear reactions N (^4S_u) + N_2 ($X^1\Sigma_g^+$, $A^3\Sigma_u^+$, and $B^3\Pi_g$). J. Mol. Struct (Teochem.) 202, 135–142 (1989)
11. Garcia, E., Laganà, A.: The largest angle generalization of the rotating bond order potential: the H + H_2 and N + N_2 reactions. J. Chem. Phys. 103, 5410–5416 (1995)
12. Laganà, A.: A rotating bond order formulation of the atom diatom potential energy surface. J. Chem. Phys. 95, 2216–2217 (1991)
13. Laganà, A., Ferraro, G., Garcia, E., Gervasi, O., Ottavi, A.: Potential energy representations in the bond order space. Chem. Phys. 168, 341–348 (1992)
14. Garcia, E., Laganà, A.: Effect of varying the transition state geometry on N + N_2 vibrational deexcitation rate coefficients. J. Phys. Chem. A 101, 4734–4740 (1997)
15. Wang, D., Stallcop, J.R., Huo, W.M., Dateo, C.E., Schwenke, D.W., Partridge, H.: Quantal study of the exchange reaction for N + N_2 using an ab initio potential energy surface. J. Chem. Phys. 118, 2186–2189 (2003)
16. Garcia, E., Saracibar, A., Gómez Carrasco, S., Laganà, A.: Modeling the global potential energy surface of the N + N_2 reaction from ab initio data. Phys. Chem. Chem. Phys. (accepted)
17. Werner, J.J., Knowles, P.J., Almlof, J., Amos, R.D., Berinng, A., Cooper, D.L., Deegan, M.J.O., Dobbyn, A.J., Eckert, F., Elbert, S.T., Hampel, C., Lindh, R., Lloyd, A.W., Meyer, W., Nicklass, A., Peterson, K., Pitzer, R., Stone, A.J., Taylor, P.R., Mura, M.E., Pulay, P., Schutz, M., Stoll, H., Thorsteinsson, T.: MOLPRO is a package of ab initio programs
18. Wang, D., Huo, W.M., Dateo, C.E., Schwenke, D.W., Stallcop, J.R.: Reactive resonances in the N + N_2 exchange reaction. Chem. Phys. Lett. 379, 132–138 (2003)
19. Bowman, J.M.: Reduced dimensionality theory of quantum reactive scattering. J. Phys. Chem. 95, 4960–4968 (1991)
20. Bowman, J.M.: Approximate time independent methods for polyatomic reactions. Lect. Notes in Chem., vol. 75, pp. 101–114 (2000)
21. Back, R.A., Mui, J.Y.P.: The reactions of active nitrogen with $N^{15}O$ and N_2^{15}. J. Phys. Chem. 66, 1362–1364 (1962)
22. Bar-Nun, A., Lifshitz, A.: Kinetics of the homogeneous exchange reaction: $^{14-14}N_2$ + $^{15-15}N_2 \rightarrow 2\ ^{14-15}N_2$. Single-pulse shock-tube studies. J. Chem. Phys. 47, 2878–2888 (1967)
23. Lyon, R.: Search for the N-N_2 exchange reaction. Can. J. Chem. 50, 1433–1437 (1972)